Chapter 6
A Novel Hybrid Magnetoacoustic Measurement Method for Breast Cancer Detection

Maheza Irna Mohamad Salim, Nugraha Priya Utama, Eko Supriyanto, Khin Wee Lai, Yan Chai Hum and Yin Mon Myint

Abstract Breast cancer is the most common cancer in women worldwide. It is a disease of uncontrolled breast cells growth, in which the cells acquire genetic alteration, causing them to proliferate more aggressively as compared to normal tissue development. In current medical practice, the gold standard for breast cancer screening is mammography. However, its usage is unsafe as it exposes patient to ionizing radiation and it is less comfortable due to the need for breast compression. Another available option for breast screening is ultrasound. To date, ultrasound is an important adjunct modality to mammography regardless of its low sensitivity in detecting small cancers from normal tissues due to overlapping ultrasonic characteristics of these tissues. To address this problem, a hybrid magnetoacoustic measurement method (HMM) that combines ultrasound and magnetism for the

M. I. Mohamad Salim (✉)
Universiti Teknologi Malaysia, Level 3, V01, Block A, Satellite Building, Skudai-Johor, Malaysia
e-mail: maheza@biomedical.utm.my

N. P. Utama · Y. M. Myint
Faculty of Biosciences and Medical Engineering, Universiti Teknologi Malaysia, Level 3, V01, Block A, Satellite Building, Skudai-Johor, Malaysia
e-mail: utama@biomedical.utm.my

Y. M. Myint
e-mail: yinmontt@gmail.com

E. Supriyanto
Faculty of Biosciences and Medical Engineering, IJN-UTM Cardiovascular Engineering Center, Universiti Teknologi Malaysia, Skudai-Johor, Malaysia
e-mail: eko@biomedical.utm.my

K. W. Lai
Biomedical Engineering Department, University Malaya, Kuala Lumpur, Malaysia
e-mail: lai.khinwee@um.edu.my

Y. C. Hum
MIMOS Berhad, Technology Park Malaysia, 57000 Kuala Lumpur, Malaysia
e-mail: yc.hum@mimos.my

K. W. Lai et al., *Advances in Medical Diagnostic Technology*,
Lecture Notes in Bioengineering, DOI: 10.1007/978-981-4585-72-9_6,

simultaneous assessment of bioelectric and acoustic profiles of breast tissue is proposed. Previous studies have shown that in cancerous tissue, changes in ultrasonic characteristics occur due to uncontrolled cell multiplication, excessive accumulation of protein in stroma, and enhancement of capillary density. Additionally, changes in conductivity also occur due to the increase in cellular water and electrolyte content, as well as membrane permeability due to increased metabolic requirements. In HMM, the interaction between the ultrasound wave and the magnetic field in the breast tissue results in Lorentz force. This produces a magnetoacoustic voltage output, which is proportional to breast tissue conductivity. Simultaneously, the ultrasound wave is sensed back by the ultrasound receiver for tissue acoustic evaluation. At the end of this study, ultrasound wave characterization results showed that normal breast tissue experienced higher attenuation compared with cancerous tissue. The mean magnetoacoustic voltage results for normal tissue were lower than the cancerous tissue group. This demonstrates that the combination of acoustic and bioelectric measurements appears to be a promising approach for diagnosis.

6.1 Introduction and Literature Review

6.1.1 Breast Cancer

Breast cancer is a disease of uncontrolled breast cells growth, in which the cells acquire a genetic alteration that allows them to multiply and grow outside the context of normal tissue development (Locasale and Cantley 2010). The cell metabolism increases to meet the requirements of rapid cell proliferation, autonomous cell growth, and cell survival (Locasale and Cantley 2010; Alberts et al. 2002).

The key aspect in diagnosis of breast cancer is to determine whether the cancer is in situ or invasive (Donegan and Spratt 2002; Moinfar 2007; Cuzick 2003). In situ cancers confine themselves to the ducts or lobules and do not spread to the surrounding organ. Two main types of in situ breast cancer are the ductal carcinoma in situ (DCIS) and lobular carcinoma in situ (LCIS). DCIS means that the abnormal cancer cells are found only at the lining of the ducts. However, it can be found in more than one place in the breast since the cancer travels through the ducts. DCIS has a high cure rate especially if given early treatments. However, it can change to invasive carcinoma without a proper treatment. LCIS means that the abnormal cancer cells are found in the lining of milk lobules and is a warning sign of increased risk of developing invasive cancers. Invasive cancer is a cancer that has penetrated through normal tissue barriers and invades the surrounding organs via the bloodstream and the lymphatic system. The most common invasive cancers are invasive lobular carcinoma and invasive ductal carcinoma. There are also some rare cancers such as the inflammatory breast cancer and Paget's disease that differ

from invasive ductal and lobular carcinoma, in which they do not form a distinct mass or lump in the breast (Donegan and Spratt 2002; Moinfar 2007).

The most common symptom of breast cancer is the presence of painless and slow growing lump that may alter the contour or size of the breast (Thomas et al. 1997). It is also characterized by skin changes, inverted nipple, and bloodstained nipple discharge (Donegan and Spratt 2002; Moinfar 2007). The lymphatic nodes under the armpit may be swollen if affected by cancer. In late stages, the growth may ulcerate through the skin and get infected (Donegan and Spratt 2002; Moinfar 2007). Bone pain, tenderness over the liver, headaches, shortness of breath, and chronic cough may be an indication of the cancer spreading to the other organs in the body (Moinfar 2007).

The main risk factor for breast cancer can be usefully grouped into four major categories (Cuzick 2003): family history or genetics, hormonal, proliferative breast benign pathology, and mammographic density. These four factors have now been thoroughly studied, and accurate quantitative estimates are available for the factors (Cuzick 2003). In terms of genetics, the mutations of BRCA1 and BRCA2 genes have been identified as genetic susceptibility of breast cancer in which carriers of the genes have at least 40–85 % chances of getting breast cancer (Cuzick 2003). Besides that, several lines of evident points to estrogen levels as a hormonal prime factor for the development of breast cancer (Cuzick 2003). The evidents include result of laboratory studies, direct measurement to postmenopausal women, and risk reduction when women take anti-estrogen (Thomas et al. 1997). However, details of mechanisms are still unclear. In addition to that, the risk of cancer following benign breast disease has also been identified. A recent study shows that benign breast disease in the absence of proliferation does not carry any excess risks (Cuzick 2003). However, a simple hyperplasia doubles the excess rate, and atypical hyperplasia increases the risk of getting breast cancer to fourfold (Cuzick 2003). In terms of mammographic density, earlier studies had clearly demonstrated that a radiographically opaque area in the mammography is an important measure of the risk of developing breast cancer.

Finally, female breast has a special place in human affairs beyond its biological function. It was a prominent feature of motherhood, beauty, fertility, and abundance since the early days. Diseases of the breast particularly cancer are not only the threats to women's health and well-being but are also attacks on femininity, nurturance, motherhood, and personal identity. Hence, efforts to improve breast cancer detection and treatment must continue not only to save lives but also as a part of the social betterment.

6.1.2 Normal and Cancerous Breast Tissue: Changes in Density and Conductivity

The mammary gland is a complex tissue that consists of epithelial parenchyma embedded in an array of stromal cell (Arendt et al. 2010). It undergoes dynamic changes over the lifetime of a woman from the expanded development at puberty,

to proliferation and apoptosis during the menstrual cycle and to full lobuloalveolar development for lactation (Donegan and Spratt 2002; Moinfar 2007; Riordan 2005). Previous studies had shown that changes in breast tissue density and conductivity occur in cancerous tissue. Breast carcinoma causes the breast cells to proliferate, grow, and pile up outside the context of normal tissue development, which finally results in increased local cell density (Locasale and Cantley 2010). In addition to that, it is well established that stroma associated with normal mammary gland development is totally different from that associated with carcinoma (Arendt et al. 2010; Bissel and Radisky 2001; Cukierman 2004; Orimo et al. 2005). Compared to normal breast tissue, the stroma accompanying breast carcinoma contains increased protein, immune cell infiltrates, and enhanced capillary density (Arendt et al. 2010). Extensive multiproteins accumulation in the stroma has also been associated with enhanced growth and invasiveness of the carcinoma (Shinoji et al. 1998; Provenzano et al. 2008). Increased collagen 1 and fibrin deposition, elevated expression of alpha smooth muscle actin (αSMA), collagen IV, prolyl-4-hydroxylase, fibroblast-activated protein (FAP), tenascin, desmin, calponin, caldesmon, and others have collectively altered the structure, stiffness, and density of the extracellular fluid (Arendt et al. 2010; Bissel and Radisky 2001; Cukierman 2004; Orimo et al. 2005). Enhanced capillary density or angiogenesis is the complex process, leading to the formation of new blood vessels from the preexisting vascular network and further increasing the compactness of the tissue (Gasparini 2001). The formation of angiogenesis is induced by the secretion of specific endothelial cell growth factors produced by the tumor or the stromal cells (Gasparini 2001). Studies have shown that angiogenesis plays an important role in facilitating further tumor progression (Chan et al. 2005; Shinoji et al. 1998).

In medical imaging, changes in breast density due to carcinoma are usually assessed using mammography and ultrasound. Mammographic density refers to the relative abundance of low-density adipose tissue to high-density glandular and fibroblastic stromal tissues within the breast. A previous study had shown that the involvement of 60 % or more of the breast with mammographically dense tissue confers threefold to fivefold increased risk of breast cancer (Cuzick 2003; Arendt et al. 2010). In ultrasonography, changes in tissue density are indicated by the changes in velocity. Ultrasound velocity increases when it travels through a dense material and decreases when it travels through a less dense material (Glide et al. 2007). The study report is in agreement with an earlier observation that shows ultrasound velocity traveling through breast carcinoma is higher than those of normal tissue (Bamber 1983).

The presented literature supports the fact of density alteration in breast carcinoma. In general, the density of mammary fat pad is 928 kg/m^3 and 1,020 kg/m^3 for normal tissue. However, due to the altered density of breast carcinoma, many researches (Fern 2007; Degen et al. 2007) estimate the density of breast carcinoma to be very close to muscle, which is 1,041 kg/m^3 (Fern 2007).

On the other hand, bioelectric measurement for human breast tissue has started since the 1920s with the measurement of excised normal and cancerous breast tissues. Compared to normal tissue, malignant tissue has higher conductivity

(Surowiec et al. 1988; Chaudary et al. 1984) and permittivity (Chaudary et al. 1984; Sha et al. 2002; Jossinet et al. 1985) and lower impedivity (Jossinet 1996). These changes are due to the increase in cellular water and electrolyte content as well as altered membrane permeability and blood perfusion (Zou and Guo 2003; Sha et al. 2002; Jossinet et al. 1985; Jossinet 1996). In terms of conductivity changes, a study by Chaudary et al. (1984) in the frequency range of 3 MHz–3 GHz showed that conductivity, σ, of malignant tissue is higher than that of normal tissue, particularly at frequencies below 100 MHz. The research reveals that σ is from 1.5 to 3 mS/cm for normal tissue and from 7.5 to 12 mS/cm for malignant tissue.

At the frequency of 20 kHz–100 MHz, comparative bioelectric study (Surowiec et al. 1988) between tumor and its peripheral tissue shows that cancerous tissue has higher conductivity, σ, than the surrounding tissue. Data from a few tumor samples indicate that σ ranges from 0.3 to 0.4 mS/cm for normal and from 2.0 to 8.0 for the central part of tumor. At 10 MHz specifically, normal tissue conductivity ranges between 0.3 mS/cm, while cancerous tissue conductivity ranges from 4 to 6 mS/cm.

From these measurements, it can be observed that there are significant differences in conductivity between the normal and malignant tissues.

6.1.3 Ultrasound in Breast Oncology Diagnostics

Breast ultrasound is an interactive breast imaging process using sound wave at the frequency of 20 kHz–200 MHz (Kremkau 2002). In the world of medical diagnostics, breast ultrasound has an established and significant role in the diagnostics of breast abnormalities (Svensson 1997). Ultrasound is superior from mammography for its non-ionizing radiation. This makes ultrasound an imaging of choice to manage symptomatic breast in younger women as well as in pregnant and lactating mother whom the radiation of mammography is pertinent (The and Wilson 1998). Ultrasonography is also a reliable modality for solid and cystic breast anomaly differentiation (Svensson 1997; Stavros et al. 1995; Sehgal et al. 2006). It is also used in imaging augmented and inflamed breast (Svensson 1997; Stavros 2004). However, in the current practice, the proportion of patient in whom breast ultrasonography is considered necessary is only 40 % (Flobbe et al. 2002). This means that ultrasonography is not indicated for the rest 60 % of patients referred for breast imaging (Flobbe et al. 2002). This practice explains major constraint of ultrasonography in breast imaging that limits its usage for the diagnostics of breast symptoms and for screening asymptomatic patients (The and Wilson 1998; Sehgal et al. 2006).

The major problem of ultrasonography is its low sensitivity in detecting small and preinvasive breast cancers (Fornage et al. 1990) from normal tissues due to the overlapping ultrasonic characteristics in these tissues (Bamber 1983; Edmonds and Mortensen 1991; Landini and Sarnelli 1986). Breast ultrasound diagnostics relies on several sonographic features that are based on margin, shape, and echotexture. Breast cancers are often characterized by poorly defined margins, irregular

borders, spiculation, marked hyperechogenicity, shadowing, and duct extension (Stavros 2004).

A systematic review on 22 independent studies to investigate the sensitivity of ultrasound in breast cancer detection was conducted by Flobbe et al. (2002). In the review, the patient population was divided into four groups, namely (1) patient undergoes mammography. Hence, ultrasound interpretation is with the knowledge to prior mammography (five studies). (2) Patient undergoes mammography and clinical examinations. Hence, interpretation is based on the previous clinical and imaging data (four studies). (3) Patients are referred for pathology and mammography. Hence, ultrasound interpretation is with the knowledge to prior mammography and pathology result (six studies), and finally, (4) ultrasound is interpreted blindly without prior patient clinical data (seven studies). The average ultrasound sensitivity for each group of patient is 82.60, 88.25, 86.83, and 82.57 %, respectively. This systematic review has revealed the weakness of ultrasound in the diagnostics of patients with breast abnormalities regardless of the existing patients' prior clinical information. The study concludes that a little evidence support was found to confirm the well-recognized value of ultrasonography in breast cancer detection. Other than the review, an independent report by Singh et al. (2008) also shows the low sensitivity of ultrasound in the detection of breast cancer.

Another limitation of ultrasound is its inability to detect microcalcification, a calcium residue found in the breast tissue as an early indicator of DCIS (Sehgal et al. 2006; Anderson et al. 2000). In ultrasonography, the presence of microcalcification in tissue is often masked by the breast tissue heterogeneity and grainy noise due to speckle phenomena (Weinstein et al. 2002; Alizad et al. 2004). The reasons make microcalcification detection with ultrasonography unreliable (Anderson et al. 2000).

Previous study (Chang et al. 2011) also reported the sensitivity of ultrasonography for breast cancer detection evaluated by three different radiologists with experienced from 8 to 16 years. The result showed that the achieved sensitivities were 66.7, 87.5, and 56.3 % for the three radiologists. This study found that breast ultrasound diagnosis was complicated not only by the low sensitivity of the ultrasound itself but also by the dependency of ultrasound result to operator. This means that a single sonographic image may be interpreted differently by different operators and the result is relative to the operator skills and experience, variations in human perceptions of the images, differences in features used in diagnosis, and lack of quantitative measures used for image analysis (Kuo et al. 2002; Horsch et al. 2004; Wen et al. 1997, 1998; Wen and Bennet 2000; Su et al. 2007; Norton 2003; Ibrahim 2005).

This inter-reader variability has led to automated ultrasonographic image evaluation via computer-aided diagnosis (CAD system). CAD is a multistep process that involves identification of lesion by segmentation, extraction, and recognition using a complex and intelligent algorithm based on echotexture, margin, and shape (Kuo et al. 2002; Horsch et al. 2004). It offers potentially accurate judgment to generate valuable second opinion in assisting diagnosis. In CAD, the area under the ROC curve is the performance metric to evaluate CAD with one representing perfect performance. Studies have shown that sonographic

CAD is able to give a good classification performance of 0.83–0.87 (Shankar et al. 2002; Sahiner et al. 2004; Dumane et al. 2002), excellent performance of 0.92 (Sahiner et al. 2004), and near-perfect performance of 0.95–0.98 (Chen et al. 2003). With the increasing acceptance of Mammo CAD and MRI CAD, sonographic CAD has also been widely accepted to assist in diagnostics. In addition to that, previous studies also reported that sonographic CAD is helpful for diagnosis (Kuo et al. 2002; Horsch et al. 2004).

Although breast ultrasound diagnosis has improved over the time, its usage in breast cancer detection is still limited due to its low detection sensitivity to breast masses and microcalcification as well as inter-reader variability. Hence, in order for ultrasound to compete with other breast imaging modalities, additional tissue properties need to be further explored for a better breast cancer detection method.

6.1.4 Lorentz Force-Based Magnetoacoustic Imaging

The earliest research in Lorentz force-based magnetoacoustic imaging was started since 1988 by the work of Towe and Islam in the development of noninvasive measurement system for bioelectric current (Towe and Islam 1988; Islam and Towe 1988). The measurement system manipulates vibrations that are produced by Lorentz force as a result of the interaction between audible-frequency oscillating magnetic field and static magnetic field on current carrying media. In this approach, oscillating magnetic excitation is employed to induce eddy current in a conductive sample, which is put in a static magnetic field. The eddy current in the static magnetic field is subjected to Lorentz force, which causes vibration that is proportional to the magnitude of the internal current in the media. The system was tested to measure a current carrying wire as well as a living hamster. The resulting vibration is at the frequency of the oscillating magnetic field, which was easily detected using microphone since it is in the range of audible frequency.

In 1994, a complete theoretical model of magnetoacoustic imaging for bioelectric current was published by Roth et al. (1994). The theoretical model is based on the fundamental equation of continuum mechanics and electromagnetism where feasibility measurement of bioelectric current in vitro and in vivo is discussed. While in vitro imaging is very promising, Roth et al. (1994) concluded that in vivo magnetoacoustic signal that is generated by the body may be overwhelmed by the ambient noise such as sounds produced by muscle contraction and fluid or gas movement and these artifacts can be reduced by increasing the frequency of the oscillating magnetic field beyond the frequency of natural body sounds.

Later in 2006, Bin He et al. improve the system that is first inspired by Towe and Islam with the development of Magneto Acoustic Tomography with Magnetic Induction (MATMI) (Li et al. 2006; Xia et al. 2007). MATMI is a two-dimensional imaging system that shares the concept of the earlier system. However, the frequency of the oscillating magnetic field used in MATMI is in the range of ultrasonic frequency. This improvement enables the system to not only reducing the body

artifacts but also producing image mapping with a resolution close to sonography (Li et al. 2006; Xia et al. 2007). MATMI was tested to image wire phantom as well as real biological tissue with different conductivity in vitro. The result shows that MATMI is capable to produce a high-resolution image and is sensitive to differentiate various types of tissue with different conductivity in the image.

In 1998, Wen et al. (1997, 1998), Wen and Bennet (2000), Wen (2000) developed Hall effect imaging, a 2D magnetoacoustic imaging system that employs different magnetoacoustic approaches. In HEI, non-focused ultrasound wave and magnetic field are combined to produce Lorentz force interaction in tissue to access tissue conductivity (Wen et al. 1997, 1998; Wen and Bennet 2000). Propagation of ultrasound wave inside the breast tissue will cause ionic charges in the breast tissue to move at high velocity due to the back and forth motion of the wave (Wen et al. 1997, 1998; Wen and Bennet 2000). Moving charges in the presence of magnetic field will experience Lorentz force. Lorentz force separates the positive and negative charges, producing an externally detectable voltage (Wen et al. 1997, 1998; Wen and Bennet 2000) that can be collected using a couple of skin electrodes (Wen et al. 1998). HEI was first tested to image a phantom made of polycarbonate that was immersed in saline solution. Later, it was tested to image biological tissue. A series of experimental studies on HEI showed that the resulting voltage was linearly proportional to the magnetic field strength and the ultrasound-induced velocity of the ionic particle.

A further study by Su et al. (2007) had improved HEI's setup when a focused ultrasound transducer was used to focus the sound wave at a focal point. This was to prevent high attenuation from occurred in tissue via ultrasound beam localization. Beam localization allowed the generation of Lorentz force interaction only at the focal point to maximize the interaction effects and increase the resulting voltage value. The ultrasound probe was attached to a 1-mm step size motor so that scanning can be done by moving the focused transducer and then 2D image can be generated. As a result, a better voltage value was obtained for the profile assessment of tissue.

Based on the review, it can be concluded that previous magnetoacoustic imaging manipulated magnetoacoustic interaction for the bioelectric profile assessment of tissue only. The output of ultrasound wave that was initially used to stimulate tissue particle motion was ignored, though it contained valuable information with regard to tissue mechanical properties. Hence, this study employs the concept of hybrid magnetoacoustic measurements, which considers the acoustic and bioelectric outputs to improve the existing breast cancer detection method.

6.1.5 Theory of Lorentz Force-Based Magnetoacoustic Imaging

Theoretically, magnetoacoustic imaging manipulates the interaction between the ultrasound wave and magnetic field in a current carrying media. Considering an ion in a breast tissue sample with charge q, a step change in conductivity σ and

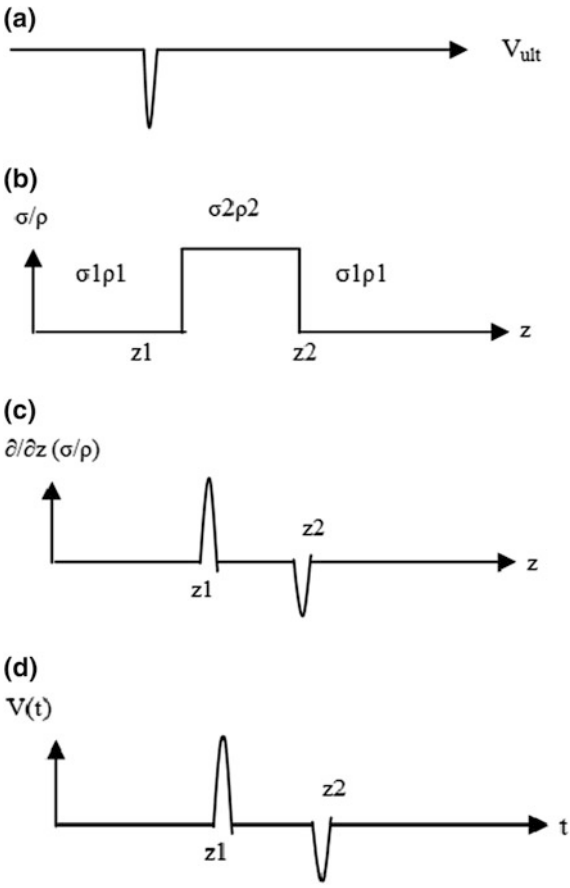

Fig. 6.1 Formation of magnetoacoustic voltage at tissue interfaces. **a** Ultrasound wave packet. **b** Step change in conductivity and density in HMM measurement chamber due to the presence of breast sample. **c** Conductivity and density gradient at tissue interfaces. **d** Magnetoacoustic voltage at tissue interfaces

density ρ occurs between positions z_1 and z_2 in the HMM measurement chamber as shown in Fig. 6.1b due to the presence of oil and breast tissue sample.

The longitudinal motion of an ultrasound wave in z direction (Fig. 6.1a) will cause the ion to oscillate back and forth in the medium with velocity $\mathbf{V_0}$. In the presence of constant magnetic field $\mathbf{B_0}$ in y direction, the ion is subjected to the Lorentz force (Wen et al. 1997, 1998; Wen and Bennet 2000).

$$\mathbf{F} = q[\mathbf{v}_z \times \mathbf{B_0}] \tag{6.1}$$

From (6.1), the equivalent electric field is (Wen et al. 1997, 1998; Wen and Bennet 2000)

$$\mathbf{E}_0 = \mathbf{v}_z \times \mathbf{B}_0. \tag{6.2}$$

The field $\mathbf{E_0}$ and current density $\mathbf{J_0}$ oscillate at the ultrasonic frequency in a direction mutually perpendicular to the ultrasound propagation path and the

magnetic field $\mathbf{B_0}$ (**x** direction). The electric current density is given by (Wen et al. 1997, 1998; Wen and Bennet 2000):

$$\mathbf{J}_0 = \sigma[\mathbf{v}_z \times \mathbf{B_0}] \tag{6.3}$$

Finally, the magnetoacoustic voltage, V, across measurement electrodes *a* and *b* due to $\mathbf{J_0}$ can be calculated by the following (Su et al. 2007; Wen 2000; Zeng et al. 2010; Renzhiglova et al. 2010):

$$\mathbf{V} = \iiint [(\mathbf{v_z} \times \mathbf{B}) \cdot \mathbf{J}_{ab}/\mathbf{I}]\mathrm{dV} \tag{6.4}$$

where $\mathbf{J}_{ab}$ is the current density that is induced under the electrodes surface in the breast tissue if a one ampere current, **I** is applied to the sample through the measurement electrodes (Zeng et al. 2010; Renzhiglova et al. 2010).

In addition to that, in ultrasound term, the amplitude of magnetoacoustic voltage in time domain is proportional to (Wen et al. 1998)

$$\mathrm{V}(t) \propto W \int_{\text{Soundpathinitial}}^{\text{Final}} \frac{\partial}{\partial z}\left[\frac{\sigma}{\rho}\right]\left[\int_0^t \partial P_z \mathrm{d}t\right]\mathrm{d}z \tag{6.5}$$

Following the equation of (6.5), gradient σ/ρ is nonzero only at interfaces z_1 and z_2 (Fig. 6.1c) giving rise to the magnetoacoustic voltage (Fig. 6.1d). The polarity of the two peaks is opposite because the σ/ρ gradients at z_1 and z_2 are in opposite direction with positive value occur at the transition of low density and conductivity area to high density and conductivity area and vice versa (Wen et al. 1997, 1998; Wen and Bennet 2000; Su et al. 2007; Wen 2000). In a uniform area within the tissue sample, the average ultrasound velocity, $\mathbf{v_0}$, is zero, and hence, no signal is observed (Wen et al. 1997, 1998; Wen and Bennet 2000).

6.2 Methodology

6.2.1 Experimental Setup

The entire experimental study was conducted in an anechoic chamber with shielding effectiveness of 18 kHz–40 GHz. Electromagnetic shielded environment is preferred to prevent external electromagnetic interference from contaminating the recorded magnetoacoustic voltage and interrupting the sensitive lock-in amplifier readings.

The HMM system consists of a 5077PR Manually Controlled Ultrasound Pulser Receiver unit, Olympus-NDT, Massachusetts, USA. The unit delivered 400 V of negative square wave pulses at the frequency of 10 MHz and PRF of 5 kHz, to 2 units of 0.125-inch standard contact, ceramic ultrasound transducers having the

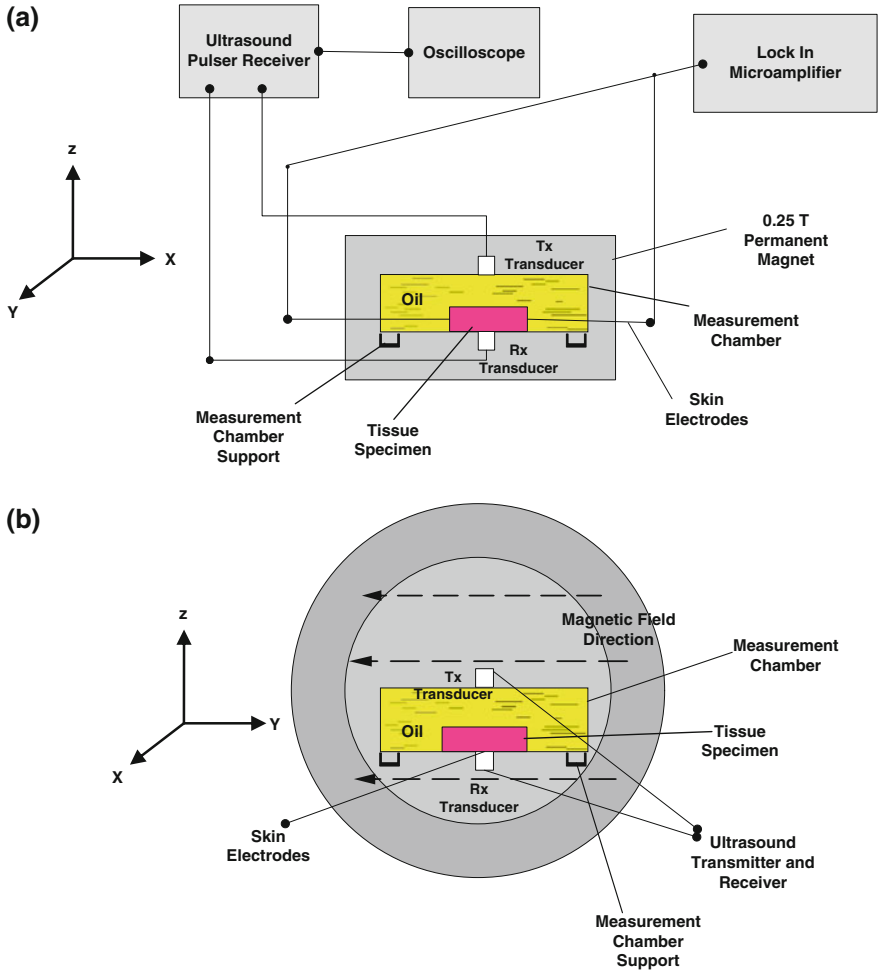

Fig. 6.2 Block diagram of the hybrid magnetoacoustic system. **a** Side view. **b** Cross-sectional view

peak frequency of 9.8 MHz. The transducers were used to transmit and receive ultrasound wave in transmission mode setting from the z direction. The pulser receiver unit was also attached to a digital oscilloscope, model TDS 3014B, Tektronix, Oregon, USA, for signal display and storage purposes.

A custom made, 15-cm height, diameter pair magnetized NdFeB permanent magnet is used to produce static magnetic field, with the intensity of 0.25T at the center of its bore. The diameter of the magnet bore is 5 cm, and the direction of magnetic field was set from the y-axis. The overall concept of HMM is shown in Fig. 6.2.

Magnetoacoustic voltage measurements were made from the x direction with respect to the measurement chamber. It was conducted using two units of custom made, ultrasensitive carbon fiber electrodes with 0.1 mm tip diameter. In general, carbon fiber electrode has been used very extensively in the in vivo (Dressman et al. 2002; Yavich and Tilhonen 2000) and in vitro including transdermal (Miller et al. 2011) bioelectrical studies of cells (Chen et al. 2011; de Asis et al. 2010) and tissue of animals (Yavich and Tilhonen 2000; Fabre et al. 1997) and humans (Crespi et al. 1995; Dressman et al. 2002; Shyu et al. 2004). On top of that, its usage in electrophysiological studies and voltammetric/amperometric analysis is perfected by its significantly less noise (Crespi et al. 1995). Furthermore, carbon fiber has a very weak paramagnetic property compared to other conventional electrodes. Due to the property, carbon fiber has been used in combination with fMRI to study the brain stimulation (Shyu et al. 2004). On top of that, carbon fiber electrode is also excellent device with greater sensitivity, selectivity and offers wide range of detectable species since its impedance can be tailored to match the sample under test (Buckshire 2008). In addition to that, many studies reported that carbon fiber electrode has the sensitivity down to 1 nV (TienWang et al. 2006; Han et al. 2004). In this study, the carbon fiber electrodes were connected to a high-frequency lock-in amplifier, model SR844, Stanford Research System, California, USA. The full-scale sensitivity of the amplifier is 100 nVrms (Stanford Research System 1997). Magnetoacoustic voltage measurement was made by touching the tip of the electrodes to the tissue in x direction.

6.2.2 Preparation of Samples

Two types of samples were used in this study. The first sample was a set of tissue mimicking gel with properties that are very close to normal breast tissue. Another sample was a set of animal breast tissues that was harvested from a group of tumor-bearing laboratory mice and its control strain shown in Fig. 6.3. The tissue mimicking gel was used in the early part of this study to understand the basic response of HMM system to linear samples before it was tested to complex samples like real tissues. The same experimental planning was also observed in previous studies (Wen et al. 1997, 1998; Wen and Bennet 2000), in which phantoms were tested to their system before they were tested on real biological tissue.

The tissue mimicking gel was prepared from a mixture of gel powder, sodium chloride (NaCl), and pure water at the right proportion to achieve the desired density and conductivity. Fifteen samples of breast tissue mimicking gel were used in this preliminary study. During the experiment, the samples were cut down to an approximately 1 cm $\times$ 1 cm size with 2-mm thickness. Thickness standardization was made using a U-shaped mold with 2-mm opening. Three random samples were chosen for a baseline density and conductivity measurement as shown in Table 6.2.

Fig. 6.3 Transgenic mice strain FVB/N-Tg MMTV-PyVT that carries high-grade invasive breast adenocarcinoma

On the other hand, the use of animal in this study was approved by the National University of Malaysia Animal Ethics Committee. Transgenic mice strains FVB/N-Tg MMTV-PyVT 634 Mul and its control strain FVB/N were obtained from the Jackson Laboratory, USA. For the transgenic mice set, hemizygote male mice were crossed to female non-carrier to produce 50 % offspring carrying the PyVT transgene.

Transgene expression of the mice strain is characterized by the development of mammary adenocarcinoma in both male and female carriers with 100 % penetrance at 40 days of age (The Jackson Laboratory 2010; Bugge et al. 1998). All female carriers developed palpable mammary tumors as early as 5 weeks of age. Male carriers also developed these tumors at later age of onset (The Jackson Laboratory 2010; Guy et al. 1992). Adenocarcinoma that arises in virgin and breeder females as well as males is observed to be multifocal, highly fibrotic and involved the entire mammary fat pad (The Jackson Laboratory 2010; Bugge et al. 1998; Guy et al. 1992). Mice carrying the PyVT transgene also show loss of lactational ability since the first pregnancy (The Jackson Laboratory 2010). Pulmonary metastases are also observed in 94 % of tumor-bearing female mice and 80 % of tumor-bearing male mice (The Jackson Laboratory 2010; Bugge et al. 1998; Guy et al. 1992). The mice female offsprings were palpated every 3 days from 12 weeks of age to identify tumors.

Individual mouse was restrained using a plastic restrainer when the tumor diameter reached 2 cm for the transgenic mice or when it reached 18 weeks of age for normal mice. Anesthesia was performed using the Ketamin/Xylazil/Zoletil cocktail dilution. 0.2 ml of the anesthetic drug was administered intravenously from the mouse tail, and an additional of 2 ml of the drug was delivered intraperitoneally for about 2 h of sleeping time. The fur around the breast area was shaven. The mammary tissue was harvested from the mice while they were sleeping. Mice were then euthanized using drug overdose method. Excised breast specimens were cut down to an approximately 1 cm × 1 cm square shape with thickness of 2 mm immediately after the surgery to maintain the tissue

Fig. 6.4 Excised normal breast tissue samples

Fig. 6.5 Excised cancerous breast tissue samples

Table 6.1 Weight variations for normal and cancerous breast tissue samples

No.	Tissue group	Weight variation mean ± std dev (g)
1	Cancerous tissue	0.257 ± 0.03
2	Normal tissue	0.225 ± 0.02

physiological activities. The tissue was carefully trimmed down to the required thickness, and the standardization was made using a custom made U-shaped mold with 2-mm opening. A total of 24 normal and 25 cancerous breast tissue specimens were used in this study. Figures 6.4 and 6.5 show the excised breast tissue specimens. In addition to that, variation in tissue weight for normal and cancerous tissue group is presented in Table 6.1.

The overall process of trimming down after excision took an average time of 6 min, and the samples were immediately immersed in measurement chamber for scanning to maintain their physiological activities. The tissue position in

Table 6.2 Baseline conductivity and density measurement result

Samples	Conductivity (S/m)	Density (kg/m^3)
Normal mice breast	0.239	1,121
Cancerous mice breast	0.547	1,319
Gel	0.270	1,114

measurement chamber was fixed using a nylon fiber. Previous literature had shown that conductivity measurement is possible to be performed on excised tissue even though the tissue physiological states changes as a function of time following excision or death (Chaudary et al. 1984; Sha et al. 2002). This is because, the termination of blood perfusion after excision leads to the changes in ion distribution between inter- and extracellular spaces (Haemmerich et al. 2002). More specifically, cessation of sodium–potassium pump activity will lead to the depolarization of the cell that results in inflow of sodium and water, which causes cell swelling (Haemmerich et al. 2002; Lambotte 1986). Furthermore, the influx of Ca^{2+} leads to swelling and rupture of mitochondria that causes cell death.

However, the time taken for those changes to be observed differs according to few factors such as temperature and tissue types (Surowiec et al. 1985; Geddes and Baker 1967). Previous studies showed that conductivity measurement is almost constant in the first hour after the tissue sample had been excised (Chaudary et al. 1984) and measurement is still possible to be made within 4 h (Surowiec et al. 1988). In HMM, the excision of mice breast samples from its domain was done while the mice were sleeping and euthanasia was only performed at the end of the excision process. After excision, the sample was trimmed to the required size and immediately scanned. The time taken from excision to scanning took an average of 6 min and based on the literature presented, it is confirmed that the original conductivity of the breast tissue is retained during the scanning process.

Later, three random samples were chosen for a baseline density and conductivity measurement. Table 6.2 shows the mean baseline conductivity and density value for every group.

6.2.3 Experimental Data Collection

The data collection stage comprises two simultaneous measurements, which are HMM ultrasound measurement and HMM magnetoacoustic voltage measurements.

In ultrasound measurement, specimens were immersed in oil that was located between the ultrasound transmitter and receiver (Mohamad Salim et al. 2010) and its position was fixed using a nylon fiber. The ultrasound transmitter emitted 9.8-MHz ultrasound wave in transmission mode. The transmission mode approach gives some advantages including less complicated data and less noise (Landini and Sarnelli 1986). The distance between the ultrasound transmitter and receiver was set constant to 6 mm. The ultrasound analysis was started and performed at a

constant temperature of 21 °C using the insertion loss method described elsewhere previously (Edmonds and Mortensen 1991; Landini and Sarnelli 1986; Mohamad Salim et al. 2010). Sonification was conducted from the z direction. Vegetable oil was used as medium for ultrasound propagation to prevent any leakage current from contaminating the measurement chamber and interfering with the HMM magnetoacoustic voltage output (Su et al. 2007).

A total of 15 gel samples were used in the early part of this study, and the measurement was taken twice for every gel sample. In addition to that, 24 normal and 25 cancerous mice breast tissue samples were also used. Measurement was repeated for five times for every biological sample at any random position on the sample surface.

Additionally, the magnetoacoustic voltage measurement was made by touching the tissue surface from the x direction using the carbon fiber electrodes. The electrodes were attached to the SR844 lock-in amplifier for signal detection and recording. The electrodes tip is the only contact point between the tissue and the detection circuit. The electrodes were manually hold to touch the tissue surface from the x direction with minimal pressure to prevent tissue dislocation from its initial position as well as to prevent measurement instability due to electrodes pressure since conductivity measurement is very sensitive to skin electrodes pressure variations. The input impedance of the lock-in amplifier was set to 1 MΩ, while the time constant was set to 3 ms. However, the experimental reading was updated every 1 s since the amplifier requires a few time constant cycle to stabilize the output reading. The recorded reading of the amplifier was equal to the average voltage of the first and second peak signals. In this study, the lock-in amplifier functions as a high precision voltage reader and a filter that detects signal as low as 100 nV at 9.8 MHz and eliminate other surrounding noises.

The gain of the SR844 lock-in amplifier is calculated by the following equation:

$$\text{Gain} = \text{Maximum scale voltage}\,(10\,\text{V})/\text{Sensitivity}.$$

Again, a total of 15 gel samples were used in the early part of this conductivity study, and the measurement was repeated twice for each gel. In addition to that, 24 normal and 25 cancerous breast tissue samples were used and measurement was repeated for five times for every biological tissue sample at any random position on the breast tissue surface at one measurement side (side 1). After the fifth measurement, the tissue orientation was changed to 180° from its initial orientation and measurement was repeated again for five times (side 2).

6.2.4 Experimental Data Analysis

The experimental data analysis stage comprises the analysis of HMM ultrasound output and HMM magnetoacoustic voltage output. In general, the HMM ultrasound output requires further processing in Matlab to find the attenuation scale of the ultrasound wave for every sample via spectral analysis. The objective of

processing the HMM ultrasound output is to calculate the power spectral density (PSD) of the signal. It involved the determination of frequency content of a waveform via frequency decomposition. The use of PSD as an estimate of ultrasound attenuation was reported in many studies previously (Edmonds and Mortensen 1991; Mohamad Salim et al. 2010). PSD of the ultrasound signal was plotted in Matlab. The attenuation scale was calculated by subtracting the log mean-squared spectrum of ultrasound signal propagating through the oil without tissue, by the log mean-squared spectrum of ultrasound signal propagating through the oil with tissue, the following equation (Mohamad Salim et al. 2010):

$$\text{Attenuation (dB)} = \log P_0 - \log P_s \tag{6.6}$$

where P_s is the mean-squared spectrum of the ultrasound signal propagating in the medium with tissue/gel sample, and P_0 is the mean-squared spectrum of ultrasound signal propagating through medium without sample. Later, the attenuation scale for the gel, normal tissue group, and cancerous tissue group was exported to Microsoft Excel for statistical analysis. The statistical analysis involved the determination of mean and standard deviation for every group.

On the other hand, the recorded magnetoacoustic voltage data was statistically analyzed to find its mean and standard deviation for every sample group (gel, normal tissue, and cancerous tissue).

Both, the ultrasound attenuation value and magnetoacoustic voltage value were fed to an artificial neural network (ANN) for breast cancer classification.

6.2.5 Development of Artificial Neural Network

In this study, an ANN with three inputs was developed for breast cancer classification. A total of 106 ultrasound data and 212 magnetoacoustic voltage data were collected during the experiment. The data were used as an input and target of the ANN. The ANN was trained using the steepest descent with momentum back-propagation algorithm in Matlab environment. The back-propagation algorithm is the most commonly used algorithm in medical computational application as experimented by many studies previously (Ibrahim 2005; Ibrahim et al. 2010). Measurement of ANN performance was made using the mean-squared error (MSE) (Ibrahim 2005; Ibrahim et al. 2010). Training is best when the ANN is capable to achieve the lowest MSE value.

In addition to that, each ANN configuration was tested using the testing group data to obtain the overall prediction accuracy at the end of each training and optimization process (Lammers et al. 2003; Subasi 2005). The aim is to measure the performance of the ANN architecture after each optimization. Using this method, the network was trained using a part of the data and the remainder was assigned as the testing and validation data.

The final process of development is the validation process. In this stage, a set of data that never been used during ANN training was introduced into the ANN for

Table 6.3 Details of ultrasound signals recorded by HMM

No.	Ultrasound signal	Quantity
1	Oil medium only	21
2	Oil medium with gel	30
3	Oil medium with normal breast tissue	106
4	Oil medium with cancerous breast tissue	106

classification. Validation process is very crucial as an assessment of ANN overfitting. Overfitting is usually indicated by low-performance accuracy of ANN to validation data. This explains that the developed ANN is not able to generalize its input and requires new training and optimization process.

6.3 Experimental Result and Discussion

6.3.1 HMM Ultrasound Output

The total number of ultrasound signals that were recorded in this experiment is presented in Table 6.3.

The signals were then further processed and analyzed in Matlab to find the attenuation level of the sound wave as it propagates through the gel and the breast tissue. Attenuation is the weakening of sound wave that is characterized by the reduction in amplitude and intensity as the wave propagates through tissue (Szabo 2004; Hendee and Ritenour 2002). It encompasses the absorption as it travels and the reflection and scattering as it encounters tissue interface and heterogeneous tissues (Szabo 2004). Attenuation of ultrasound is dependent to its frequency (Edmonds and Mortensen 1991; Landini and Sarnelli 1986) as higher-frequency ultrasound experiences more attenuation as compared to lower-frequency ultrasound. In this study, the attenuation of ultrasound propagating through a material in a medium was calculated using the insertion loss method (Edmonds and Mortensen 1991; Landini and Sarnelli 1986). In the insertion loss method, the attenuation of material under test is determined by subtracting the energy of ultrasound traveling through the medium with the energy of ultrasound traveling through the medium with material under test.

Figure 6.6 shows the example of ultrasound data that was recorded in this study. The signal was converted to frequency domain using the fast Fourier transform (FFT) algorithm. After signal conditioning, the mean-squared spectrum of the ultrasound signal was determined, and finally, the PSD was calculated by converting the mean-squared spectrum to its corresponding log value. An example of a PSD plot of the ultrasound signal is shown in Fig. 6.7.

The processes described above were repeated for all ultrasound signals according to their group. Then, the corresponding mean and standard deviation of attenuation for each group were calculated. The final attenuation value was

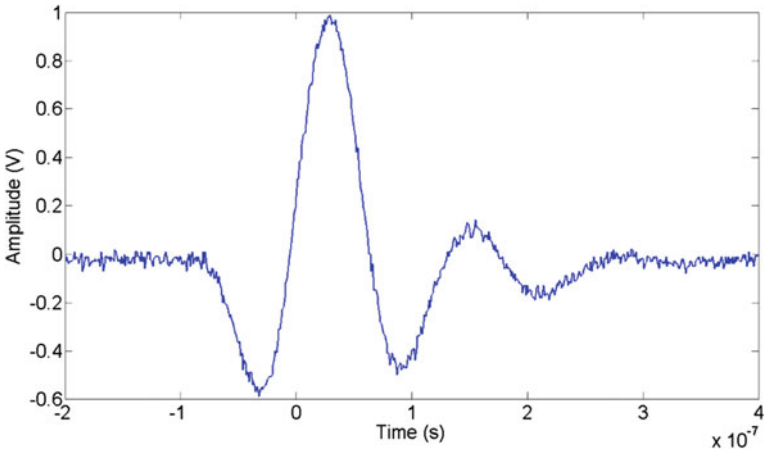

Fig. 6.6 One-dimensional ultrasound wave recorded by HMM system

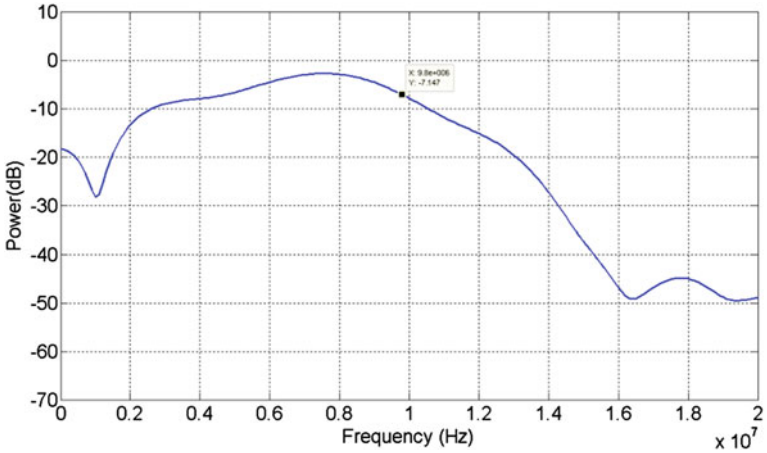

Fig. 6.7 PSD of the recorded ultrasound signal

calculated by subtracting the mean of PSD of the oil medium at 9.8 MHz by the PSD of the oil medium with the material under test (gel, normal tissue, and cancerous tissue) at 9.8 MHz.

Table 6.4 shows the final result of ultrasound attenuation scale for each group.

Absorption, scattering, and reflection are the processes that contribute to ultrasound energy attenuation in tissue. Often, the resulting attenuation is a collective result of the three processes. However, many studies reported that absorption is the most dominant factor contributing to attenuation of ultrasound wave in biological tissue via the relaxation energy loss (Kremkau 2002; Johnson et al. 2007; Berger et al. 1990).

Table 6.4 Attenuation scale of hybrid magnetoacoustic method

Type of sample	Attenuation scale ($dBmm^{-1}$) mean ± std dev
Tissue mimicking gel	0.501 ± 0.440
Normal breast tissue	2.329 ± 1.103
Cancerous breast tissue	1.760 ± 1.080

From the result, it can be observed that the tissue mimicking gel attenuates 0.501 ± 0.440 dB mm^{-1} of ultrasound energy, which is very small compared to the attenuation of real biological tissue group. The tissue mimicking gel is an ideal representation of tissue with linear behavior. In this study, the gel is designed to have the same density with normal tissue but to differ in its internal structure. The gel structure is homogenous, while the real breast tissue is heterogenous. The homogenous gel structure prevents energy losses due to scattering and reflection inside the gel. Hence, more ultrasound energy is likely to be preserved, and the observed standard deviation of the attenuation is also smaller compared to real biological tissue due to the structural homogeneity. However, major factor of attenuation in gel is still contributed by the absorption process.

From the real biological tissue result, it is observed that normal breast tissue attenuates ultrasound energy at the highest rate followed by the cancerous breast tissue. Similar to the gel, absorption process is a major factor that contributes to attenuation in real breast tissue samples. In general, breast tissue can be regarded as an arrangement of elastic and viscous components that consist of an aggregate of cells suspended by a viscous extracellular matrix (Kelley and McGough 2009). Extracellular matrix is usually modeled as aqueous solution of elastic polymers, which posses both solid and viscous properties (Alberts et al. 2002; Kelley and McGough 2009; Lim et al. 2000). Individual cells are modeled as elastic membranes containing viscous cytoplasm (Alberts et al. 2002; Lim et al. 2000). Overall, the resulting structure is viscoelastic materials (Alberts et al. 2002; Kelley and McGough 2009). In the case of breast tissue, normal breast is considered to be viscoelastic. Cancerous breast tissue that is used in this study is highly fibrotic resulting in a more elastic and denser tissue (The Jackson Laboratory 2010; Bugge et al. 1998; Guy et al. 1992; Provenzano et al. 2008). The cellular arrangements of normal and cancerous breast tissue in this study are shown in Figs. 6.8 and 6.9. The figure shows that normal cells are arranged in low density compared to the cancerous cells. Furthermore, cancerous cells have abundant protein fiber and blood vessels that further increase its density. Higher density tissue has higher inertia and resists displacement and acceleration that are caused by the ultrasound wave at its resting state (Kremkau 2002; Hendee and Ritenour 2002; Norton and Karczub 2003). Hence, it possesses very small displacement when induced by the ultrasound and quickly returns to its original equilibrium position (Hendee and Ritenour 2002; Norton and Karczub 2003). Compared to a more elastic cancerous tissue, viscoelastic molecules in normal tissue have more freedom of motion and are capable to have larger displacement and longer oscillation when induced with ultrasound. Hence, when a sound wave travels through a viscoelastic media like normal tissue,

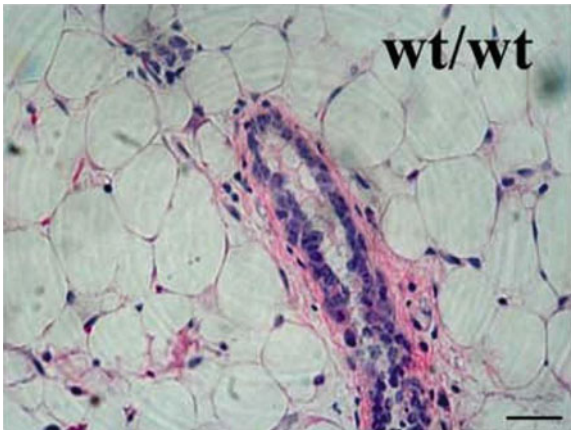

Fig. 6.8 Morphology of mammary gland from a 10-week-old normal mice model at 25 μm (Provenzano et al. 2008)

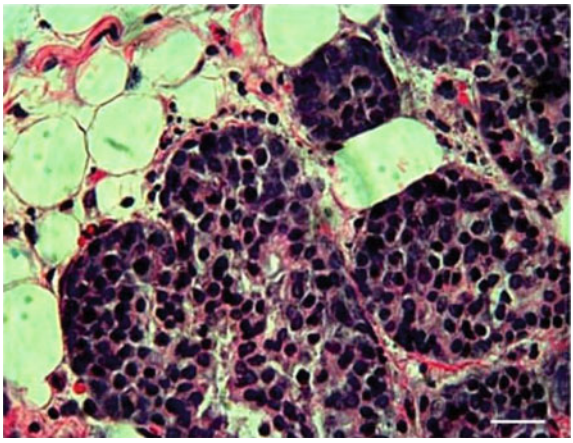

Fig. 6.9 Morphology of a high-density cancerous mammary gland of a MMTV-PyVT mice model with abundant protein fibers at 25 μm scale (Provenzano et al. 2008)

molecules vibrate for a longer period of time. This vibration requires energy that is provided to the medium by the ultrasound source. During the vibration, as the molecules attain the maximum displacement from their equilibrium, their motion stops and their kinetic energy are transformed into a potential energy associated with the position in compression zone. From this position, the molecules begin to move into the opposite direction and the potential energy is gradually transformed into kinetic energy. The conversion of kinetic to potential energy is always accompanied by energy dissipation especially when it involves larger displacement and longer oscillation such as in normal tissue. Therefore, the energy of ultrasound beam is reduced in a higher rate as it passes the viscoelastic normal tissue compared to the elastic cancerous tissue (Hendee and Ritenour 2002; Norton and Karczub 2003).

Another factor of attenuation is the reflection process that occurs at the interface between the oil and tissue. The amount of reflection at the interface is determined by the acoustic impedance difference between the oil and its adjacent medium. The

average reflection coefficient that is calculated at the oil–tissue interface varied between 0.725 and 3.35 % with the highest reflection occurred at the oil–cancerous tissue interface and the lowest reflection occurred at the oil–normal tissue interface with the acoustic impedance z, as 1.45 MRayls for oil (Johnson-Selfridge and Selfridge 1985), 1.72 MRayls for normal tissue, and 2.1 MRayls for highly fibrotic cancerous tissue.

In addition to that, the heterogeneity of the breast tissue encourages further energy losses due to scattering (Kremkau 2002; Hendee and Ritenour 2002; Norton and Karczub 2003). In cancerous tissue for instance, the structural heterogeneity is contributed not only by the cellular difference, but also by the differences in the tumor region. The tumor center usually comprises necrotic tissue area that is more homogenous and becomes more heterogenous toward the outer tissue boundary. In some cases, the necrotic area is composed of an island of fluid-like structure that is characterized by its low attenuating properties but has ten times the conductivity of normal breast tissue (Wen et al. 1997, 1998; Wen and Bennet 2000). This complex cellular and tissue heterogeneity had caused the standard deviation of the calculated attenuation scale to be high for both tissue groups.

The obtained result also shows that the attenuation scale of normal and cancerous tissue is overlapping, making the detection of breast cancer using acoustic properties alone to be difficult. This result is also in agreement with a previous study that reported on the attenuation of breast cancer in human breast tissue (Edmonds and Mortensen 1991; Landini and Sarnelli 1986).

6.3.2 HMM Magnetoacoustic Voltage Output

The magnetoacoustic voltage output measurements involve detection of as low as 0.1 μV signal at the frequency of 9.8 MHz using the carbon fiber electrodes and lock-in amplifier in the x direction. The total number of magnetoacoustic voltage signals that were recorded in this experiment is presented in Table 6.5.

The magnetoacoustic voltage reading for each group was statistically analyzed to find its mean and standard deviation. The result is presented in Table 6.6.

From the table, it is observed that cancerous tissue group produces the highest magnetoacoustic voltage range, followed by the gel group and finally the normal tissue group. This is due to a few reasons that include ultrasound attenuation level in the tissue and the conductivity of the tissue. In general, it is noted from the ultrasound measurement result that normal tissue group attenuates the highest ultrasound energy. In the case of large amount of attenuation, the sound energy that is left to move the particles in the tissue decreases. Hence, the resulting particle velocity is reduced and consequently, the value of magnetoacoustic voltage is also lower. In addition to that, the conductivity of cancerous tissue group is also higher than the normal and the gel group. Therefore, high conductivity factor contributes further to increase the value of magnetoacoustic voltage of cancerous tissue. This result proves that the resulting magnetoacoustic voltage is

Table 6.5 Total number of magnetoacoustic voltage signal recorded by HMM

No.	Magnetoacoustic voltage signal	Quantity
1	Tissue mimicking gel	30
2	Normal breast tissues (1 and 2)	212
3	Cancerous breast tissues (1 and 2)	212

Table 6.6 Magnetoacoustic voltage of HMM at 9.8 MHz

Magnetoacoustic voltage	Value (μV) mean ± std dev
Tissue mimicking gel	0.56 ± 0.21
Normal breast tissues (1 and 2)	0.42 ± 0.16
Cancerous breast tissues (1 and 2)	0.80 ± 0.21

Table 6.7 Conductivity and density data of HMM specimens

Samples	Conductivity S/m	Density kg m^{-3}	σ/ρ
Normal mice breast	0.239	1,121	$2.13e^{-4}$
Cancerous mice breast	0.547	1,319	$4.14e^{-4}$
Phantom	0.27	1,114	$2.42e^{-4}$

not absolutely related to the tissue conductivity, but also weighted by the tissue density and uniformity that influenced the ultrasound attenuation level as explained by Eq. (6.5) (Wen et al. 1997, 1998; Wen and Bennet 2000).

$$V(t) \propto w \int_{\text{Soundpath initial}}^{\text{Final}} \frac{\partial}{\partial z}\left[\frac{\sigma}{\rho}\right]\left[\int_0^t \partial P_z dt\right] dz \tag{6.7}$$

Table 6.7 summarizes the measured conductivity and density of HMM specimens along with the calculated σ/ρ as shown in Eq. (6.7) for comparison. The measurement results are in agreement with the experimental result in Table 6.7. The calculated σ/ρ value is the highest for the cancerous tissue, followed by the tissue mimicking phantom and finally the normal tissue.

From the presented results, it has been demonstrated that magnetoacoustic voltage gives information that is related to spatial information of tissue specifically the relative amplitude of conductivity changes across interface (Wen et al. 1997, 1998; Wen and Bennet 2000; Zeng et al. 2010; Renzhiglova et al. 2010). However, information inside the tissue cannot be obtained due to the oscillatory nature of ultrasound velocity that renders the signal to zero (Wen et al. 1997, 1998; Wen and Bennet 2000; Su et al. 2007).

The unique experimental result between specimen groups shows the potential of magnetoacoustic voltage parameter to be used in breast imaging.

Table 6.8 Classification result of the neural network

Data	Testing data		Validation data	
	Normal	Malignant	Normal	Malignant
Actual data	28	27	10	10
ANN result	25	25	8	10
% Group accuracy	89.29	92.59	80	100
% Total accuracy	90.94		90	

6.3.3 Artificial Neural Network (ANN) for Breast Cancer Classifications

All the ultrasound attenuation and magnetoacoustic voltage data that were collected and analyzed in this study were fed to an artificial neutral network for breast cancer classification and performance measurement of HMM system. The ANN was trained using the steepest descent with momentum back-propagation algorithm in Matlab environment. ANN with architecture of 3-2-1 (3 network inputs, 2 neurons in the hidden layer, 1 network output) with the learning rate of 0.3, iteration rate of 20,000, and momentum constant of 0.3 was used for classifications of breast cancer in this study.

The final classification performance of the optimum ANN for testing and validation data is shown in Table 6.8. The result indicates that the ANN is capable to achieve 90.94 and 90 % classification result for testing and validation data. This result shows the advantages of HMM output in providing additional bioelectric parameter of tissue instead of only acoustic properties for breast cancer diagnosis consideration. The system's high percentage of accuracy shows that the output of HMM is very useful in assisting diagnosis. This additional capability is hoped to improve the existing breast oncology diagnosis. However, the result of one-dimensional HMM can be further improved using 2D HMM where the classification is made to be image based rather than signal based.

6.4 Conclusion

At the end of this study, a hybrid tissue measurement method that is based on the combination of ultrasound and magnetism has been successfully developed. Compared to other conventional imaging methods such as MRI and mammography that manipulate only one property of tissue, the HMM system is capable to access the acoustic and electric properties of breast tissue for breast cancer evaluation. HMM produces two simultaneous outputs: the magnetoacoustic voltage that is related to tissue conductivity and the ultrasound attenuation scale that gives information related to tissue acoustic property. The system comprises a 400 V ultrasound pulser receiver unit, 9.8 MHz ultrasound transducer, 0.25T permanent

magnet, 200 MHz lock-in microamplifier, and ultrasensitive carbon fiber skin electrodes that are capable to detect magnetoacoustic voltage down to 0.1 μV.

A series of in vitro experimental study to tissue mimicking phantom as well as to real mice breast tissue harvested from tumor-bearing mice model shows that HMM is competent to access the acoustic and electric properties of not only a simple tissue mimicking phantom, but also a complex real biological tissue. The results show that normal breast tissues experience higher attenuation (2.329 ± 1.103 dB mm^{-1}) compared to cancerous tissue (1.76 ± 1.08 dB mm^{-1}). In addition to that, mean magnetoacoustic voltage results for normal tissue and cancerous tissue group are 0.42 ± 0.16 and 0.8 ± 0.21 μV, respectively. The output of HMM was further automated to develop a breast cancer diagnosis system by employing the ANN. The ANN is defined by architecture 3-2-1, with the learning rate of 0.3, iteration rate of 20,000, and momentum constant of 0.3. The final ANN accuracies to testing and validation data are 90.94 and 90 %, respectively. The system's high percentage of accuracy shows that it is very useful in assisting diagnosis.

In practice, the developed one-dimensional HMM system is not yet capable to be used for in vivo imaging. Hence, further development of the system is very crucial so that this safe and non-ionizing imaging concept can be implemented in assisting breast diagnosis.

References

Alberts B, Johnson A, Lewis J, Raff M, Roberts K, Walter P (2002) Molecular biology of the cell, 4th edn. Garland Science, New York

Alizad A, Fatemi M, Wold LE, Greenleaf JF (2004) Performance of vibro-acoustography in detecting microcalcifications in excised human breast tissue: a study of 74 tissue samples. IEEE Trans Med Imag 23:307–312

Anderson ME, Soo MSC, Trahey GE (2000) Optimizing visualization for breast microcalcifications. In: 2000 IEEE ultrasonic symposium, IEEE, San Juan, Puerto Rico, pp 1315–1320, 22–25 Oct 2000

Arendt ML, Rudnick JA, Keller PJ, Kuperwasser C (2010) Stroma in breast development and disease. In: Seminar in cell and developmental biology, vol 21. Academic Press, London, pp 11–18

Bamber JC (1983) Ultrasonic propagation properties of the breast in ultrasonic examination of the breast. In: Jellins J, Kobayashi T (eds) Ultrasonic examination of the breast. Wiley, Chichester

Berger G, Laugier P, Thalabard JC, Perrin J (1990) Global breast attenuation: control group and benign breast diseases. Ultrason Imaging 12:47–57

Bissel MJ, Radisky D (2001) Putting tumors in context. Nat Rev Cancer 1:46–54

Buckshire MJ (2008) An overview of carbon fiber electrodes used in neurochemical monitoring. Master Thesis, University of Pittsburgh

Bugge TH, Lund LR, Kombrink KK, Nielsen BS, Holmback K, Drew AF, Flick MJ, Witte DP, Dano K, Degen JL (1998) Reduced metastasis of polyoma virus middle T antigen-induced mammary cancer in plasminogen- deficient mice. Oncogene 16(24):3097–3104

Chan JK, Magistris A, Loizzi V, Lin F, Rutgers J, Osann K, DiSaia PJ, Samoszuk M (2005) Mast cell density, angiogenesis, blood clotting, and prognosis in women with advanced ovarian cancer. Gynecol Oncol 99:20–25

Chang JM, Moon WK, Cho N, Park JS, Kim SJ (2011) Radiologist's performance in the detection of benign and malignant masses with 3D automated breast ultrasound (ABUS). Eur J Radiol 78:99–103

Chaudary SS, Mishra RK, Swarup A, Thomas JM (1984) Dielectric properties of normal and malignant human breast tissue at microwave and radiowave frequencies. Indian J Biochem Biophys 21:76–79

Chen CM, Chou YH, Han KC, Hung GS, Tiu CM, Chiou HJ (2003) Breast lesions on sonograms: computer-aided diagnosis with nearly setting-independent features and artificial neural networks. Radiology 226:504–514

Chen S, Hou H, Harnische F, Patil SA (2011) Electrospun and solution blown three dimensional carbon fiber nonwoven for application as electrodes in microbial fuel cells. Energy Environ Sci 4:1417–1421

Crespi F, England T, Ratti E, Trist DG (1995) Carbon fibre micro-electrodes for concomitant in vivo electrophysiological and voltammetric measurements: no reciprocal influences. Neurosci Lett 188:33–36

Cukierman E (2004) A visual quantitative analysis of fibroblastic stromagenesis in breast cancer progression. J Mammary Gland Biol Neoplasia 9:311–324

Cuzick J (2003) Epidemiology of breast cancer—selected highlights. The Breast 12:405–411

de Asis ED, Leung J, Wood S, Nguyen CV (2010) Empirical study of unipolar and bipolar configurations using high resolution single multi-walled carbon electrodes for electrophysiological probing of electrically excitable cells. Nanotechnology 21(12):125101

Degen M, Brellier F, Kain R, Ruiz C, Terracciano L, Orend G (2007) Tenascin-W is a novel marker for activated tumor stroma in low-grade human breast cancer and influences cell behavior. Cancer Res 67:9169–9179

Donegan WL, Spratt JS (2002) Cancer of the breast, 5th edn. Saunders, Philadelphia

Dressman SF, Peters JL, Michael AC (2002) Carbon fiber microelectrodes with multiple sensing elements for in vivo voltammetry. J Neurosci Methods 119:75–81

Dumane VA, Shankar PM, Piccoli CW, Reid JM, Forsberg F, Goldberg BB (2002) Computer aided classification of masses in ultrasonic mammography. Med Phys 29:1968–1973

Edmonds PD, Mortensen CL (1991) Ultrasonic tissue characterization for breast biopsy specimen. Ultrason Imaging 13(2):162–185

Fabre B, Burlet S, Cespuglio R, Bidan G (1997) Voltammetric detection of NO in the rat brain with an electronic conducting polymer and Nafion bilayer coated carbon fiber electrodes. J Electroanal Chem 426:75–83

Fern AJ (2007) Breast cancer treatment by focus microwave thermotherapy. Jones and Bartlette Learning, Cambridge

Flobbe K, Nelemans PJ, Kessels AGH, Beets GL, Von Meyenfeldt MF, Van Engelshoven JMA (2002) The roll of ultrasonography as an adjunct to mammography in the detection of breast cancer: a systematic review. Eur J Cancer 38:1044–1052

Fornage BD, Sneige N, Faroux MJ, Andry E (1990) Sonographic appearance and ultrasound guided fine needle aspiration biopsy of breast carcinomas smaller than 1 cm^3. J Ultrasound Med 9:559–568

Gasparini G (2001) Clinical significance of determination of surrogate markers of angiogenesis in breast cancer. Crit Rev Oncol Hematol 37:97–114

Geddes LA, Baker LE (1967) The specific resistance of biological materials—a compendium of data for engineer and physiologist. Med Biol Eng Comput 5:271–293

Glide C, Duric N, Littrup P (2007) Novel approach to evaluating breast density utilizing ultrasound tomography. Med Phys 34(2):744–753

Guy CT, Cardiff RD, Muller WJ (1992) Induction of mammary tumors by expression of polyomavirus middle T oncogene: a transgenic mouse model for metastatic disease. Mol Cell Biol 12(3):954–961

Haemmerich D, Ozkan OR, Tsai JZ, Staelin ST, Tungjitkusolmun S, Mahvi DM, Webster JG (2002) Changes in electrical resistivity of swine liver after occlusion and post mortem. Med Biol Eng Comput 40:29–33

Han X, Wang CT, Bai J, Chapman ER, Jackson MB (2004) Transmembrane segments of syntaxin line the fusion pore of Ca^{2+}-triggered exocytosis. Science 304:289–292
Hendee WR, Ritenour ER (2002) Medical imaging physics, 4th edn. Wiley Liss, New York
Horsch K, Giger ML, Vyborny CJ, Venta LA (2004) Performance of computer aided diagnosis in the interpretation of lesion on breast sonography. Acad Radiol 11:272–280
Ibrahim F (2005) Prognosis of dengue fever and dengue hemorrhagic fever using bioelectrical impedance. Ph.D. Thesis, Department of Biomedical Engineering, Faculty of Engineering, University of Malaya
Ibrahim F, Faisal T, Mohamad Salim MI, Taib MN (2010) Non invasive diagnosis of risk in dengue patients using bioelectrical impedance analysis and artificial neural network. Med Biol Eng Comput 48:1141–1148
Islam MR, Towe BC (1988) Bioelectric current image reconstruction from magneto-acoustic measurements. IEEE Trans Med Imaging 7(4):386–391
Johnson SA, Abbott T, Bell R, Berggren M, Borup D, Robinson D, Wiskin J, Olsen S, Hanover B (2007) Non-invasive breast tissue characterization using ultrasound speed and attenuation—in vivo validation. In: Acoustical imaging. Springer, Berlin, pp 147–154
Johnson-Self-ridge P, Selfridge RA (1985) Approximate materials properties in isotropic materials. IEEE Trans Ultrason Ferroelectr Freq Control SU-32:381
Jossinet J (1996) Variability of impedivity in normal and pathological breast tissue. Med Biol Eng Comput 34:346–350
Jossinet J, Lobel A, Michoudet C, Schmitt M (1985) Quantitative technique for bio-electrical spectroscopy. J Biomed Eng 7:289–294
Kelley JF, McGough RJ (2009) Fractal ladder models and power law wave equation. J Acoust Soc Am 126(4):2072–2081
Kremkau FW (2002) Diagnostic ultrasound principles and instruments, 6th edn. Saunders, Philadelphia
Kuo WJ, Chang RF, Moon WK (2002) Computer aided diagnosis of breast tumors with different US system. Acad Radiol 9:793–799
Lambotte L (1986) Cellular swelling and anoxic injury of the liver. Eur Surg Res 18:224–229
Lammers RI, Hudson DL, Seaman ME (2003) Prediction of traumatic wound infection with a neural network-derived decision model. Am J Emerg Med 21(1):1–7
Landini L, Sarnelli S (1986) Evaluation of the attenuation coefficient in normal and pathological breast tissue. Med Biol Eng Comput 24:243–247
Li X, Xu Y, He B (2006) A phantom study of magnetoacoustic tomography with magnetic induction (MAT-MI) for imaging electrical impedance of biological tissue. J Appl Phys 99(6):066112
Lim CT, Zhou EH, Quek ST (2000) Mechanical model for living cell: a review. J Biomech 39:195–216
Locasale JW, Cantley LC (2010) Altered metabolism in cancer. BMC Biol 88:88
Miller PR, Gittard SD, Edward TL, Lopez DM, Xiao X (2011) Integrated carbon fiber electrodes within hollow polymer microneedles for transdermal electrochemical sensing. Biomicrofluidics 5–013415:1–14
Mohamad Salim MI, Ahmmad SNZ, Rosidi B, Ariffin I, Ahmad AH, Supriyanto E (2010) Measurements of ultrasound attenuation for normal and pathological mice breast tissue using 10 MHz ultrasound wave. In: Proceeding of the 3rd WSEAS international conference on visualization, imaging and simulation (VIS'10), WSEAS, Faro, Portugal, pp 118–122, 3–5 Nov 2010
Moinfar F (2007) Essentials of diagnostic breast pathology: a practical approach. Springer, New York
Norton SJ (2003) Can ultrasound be used to stimulate nerve tissue? Biomed Eng Online 2:1–9
Norton M, Karczub D (2003) Fundamentals of noise and vibration analysis for engineer, 2nd edn. Cambridge Press, Cambridge

Orimo A, Gupta PB, Sgroi DC, Arenzana-Seisdedos F, Delaunay T, Naeem R (2005) Stromal fibroblast presents in invasive human breast carcinomas promotes tumor growth and angiogenesis through elevated SDF-1/CXCL 12 secretions. Cell 121:335–348

Provenzano PP, Inman DR, Eliceiri KW, Knittel JG, Yan L, Rueden CT, White JG, Keely PJ (2008) Collagen density promotes mammary tumor initiation and progression. BMC Med 6(11):1–15

Renzhiglova E, Ivantsiv V, Xu Y (2010) Difference frequency magneto-acousto-electrical tomography (DF-MAET): application of ultrasound induced radiation force to imaging electrical current density. IEEE Trans Ultrason Ferroelectr Freq Control 57(11):2391–2402

Riordan J (2005) Breastfeeding and human lactation, 3rd edn. Jones and Bartlett learning, Massachusetts

Roth BJ, Basser PJ, Wiksowo JP (1994) A theoretical model for magneto-acoustic imaging of bioelectric currents. IEEE Trans Biomed Eng 41(8):723–728

Sahiner B, Chan HP, Roubidoux MA, Helvie MA, Hadjiiski LM, Ramachandran A (2004) Computerized characterization of breast masses on three-dimensional ultrasound volumes. Med Phys 31:744–754

Sehgal CM, Weinstein SP, Arger PH, Conant EF (2006) A review of breast ultrasound. J Mammary Gland Biol Neoplasia 11:113–123

Sha L, Ward ER, Story B (2002) A review of dielectric properties of normal and malignant breast tissue. In: Proceeding of IEEE SoutheastCon 2002, IEEE, pp 457–462

Shankar PM, Dumane VA, Piccoli CW, Reid JM, Forsberg F, Goldberg BB (2002) Classification of breast masses in ultrasonic B mode images using a compounding technique in the Nakagami distribution domain. Ultrasound Med Biol 28:1295–1300

Shinoji M, Hancock WW, Abe K, Micko C, Casper KA, Baine RM (1998) Activation of coagulation and angiogenesis in cancer: immunohistochemical localization in situ of clotting proteins and vascular endothelial growth factor in human cancer. Am J Pathol 152(2):399–411

Shyu BC, Lin CY, Sun JJ, Sylantyev S, Chang C (2004) A method for direct thalamic stimulation in fMRI studies using a glass-coated carbon fiber electrode. J Neurosci Methods 137:123–131

Singh K, Azad T, Dev Gupta G (2008) The accuracy of ultrasound in diagnosis of palpable breast lump. JK Sci 10(4):186–188

Stanford Research System (1997) User's manual, SR844 RF lock in amplifier, USA

Stavros AT (2004) Breast ultrasound. William and Wilkins, Philadelphia

Stavros AT, Thickman D, Rapp CL, Dennis MA, Parker SH, Sisney GA (1995) Solid breast nodules: use of sonography to distinguish between benign and malignant lesions. Radiology 196:132–134

Su Y, Haider S, Hrbek A (2007) Magnetoacousto electrical tomography, a new imaging modality for electrical impedance. In: Proceeding of 13th international conference on electrical bioimpedance and the 8th conference on electrical impedance tomography IFMBE. Springer, Graz, Austria, pp 292–295, Aug 29–Sept 2007

Subasi A (2005) Automatic recognition of alertness level from EEG by using artificial neural network and wavelet coefficient. Expert Syst Appl 28:701–711

Surowiec A, Stuchly SS, Swarup A (1985) Radiofrequency dielectric properties of animal tissue as a function of time following death. Phys Med Biol 30(10):1131–1141

Surowiec AJ, Stuchly SS, Barr JB, Swarup A (1988) Dielectric properties of breast carcinoma and the surrounding tissue. IEEE Trans Biomed Eng 35:257–263

Svensson WE (1997) A review of the current status of breast ultrasound. Eur J Ultrasound 6:77–101

Szabo TL (2004) Diagnostic ultrasound imaging: inside out. Academic Press, London

The Jackson Laboratory (2010) JAX Mice Database: MMTV-PyVT strain, USA

The W, Wilson ARM (1998) The role of breast ultrasound in breast cancer screening. A consensus statement by the European group for breast cancer screening. Eur J Cancer 34(4):449–450

Thomas HV, Reeves GK, Key T (1997) Endogenous estrogens and postmenopausal breast cancer: a quantitative review. Cancer Causes Control 8:992–998

TienWang C, Bai J, Chang PY, Chapman ER, Jackson MB (2006) Synaptotagmin–Ca^{2+} triggers two sequential steps in regulated exocytosis in rat PC12 cells: fusion pore opening and fusion pore dilation. J Physiol 570(2):295–307

Towe BC, Islam MR (1988) A magneto acoustic method for the noninvasive measurement of bioelectric current. IEEE Trans Biomed Eng 35(10):892–894

Weinstein SP, Seghal CM, Conant EF, Patton JA (2002) Microcalcifications in breast tissue phantoms visualized with acoustic resonance coupled with power Doppler US: initial observations. Radiology 224:265–269

Wen H (2000) Feasibility of biomedical application of Hall Effect imaging. Ultrason Imag 22:123–136

Wen H, Bennet E (2000) The feasibility of Hall Effect imaging in humans. In: 2000 IEEE ultrasonic symposium, San Juan, Puerto Rico: IEEE. pp 1619–1622, 22–25 Oct 2000

Wen H, Bennett E, Shah J, Balaban RS (1997) An imaging method using ultrasound and magnetic field. In: Proceeding of the 1997 IEEE ultrasonic symposium. Toronto, Ontario, IEEE, pp 1407–1410, 5–8 Oct 1997

Wen H, Shah J, Balaban RS (1998) Hall Effect imaging. IEEE Trans Biomed Eng 45:119–124

Xia R, Li X, He B (2007) Magnetoacoustic tomography of biological tissue with magnetic induction. In: Joint meeting of the 6th international symposium on noninvasive functional source of the brain and heart and the international conference on functional biomedical imaging 2007, IEEE, Hangzhou, China, pp 287–287, 12–14 Oct 2007

Yavich L, Tilhonen J (2000) In vivo voltammetry with removable carbon fiber electrodes in freely moving mice: dopamine release during intracranial self stimulation. J Neurosci Method 104:55–63

Zeng X, Liu G, Xia H, Xu X (2010) An acoustic characteristics study of magneto-acousto-electrical tomography: a new method to reconstruct current density distribution at every point of a sample. In: 2010 3rd international conference on biomedical engineering and informatics, IEEE, Yantai, pp 95–98, 16–18 Oct 2010

Zou Y, Guo Z (2003) A review of electrical impedance techniques for breast cancer detection. Med Eng Phys 25:79–90